affect the quantitative accuracy of the results, the wide-ranging successes of molecular mechanics methods suggest that they are not sources of serious error.

The calculations of energy changes based on molecular mechanics implicitly assume that the process occurs in the gas phase. The presence of the solvent might alter the relative energies of different conformations of the free ligand or in the complex, but the energies associated with these changes would be small. The major differences in $\Delta E_T$ would arise from the fact that both the ligand and the $Cr(CO)_5$ fragment would be surrounded by solvent molecules, with which there would be weakly attractive van der Waals interactions. For complex formation to occur, some portion of this solvent sheath must be removed, to expose the fraction of the surface necessary to permit the Cr-P bond to form. The $Cr(CO)_5$ fragment is in fact a strong Lewis acid, and is known to bind even such weakly basic solvent molecules as hexane with enthalpies of interaction on the order of 10 kcal $mol^{-1}$.[10b] This term, however, is a constant for the series as the ligand varies, and so need not concern us in this discussion.

The same variations in van der Waals attractive interactions that operate between the ligand and $Cr(CO)_5$ as the ligand grows larger and more complex operate also in the interactions between the ligand and solvent molecules. Thus, the energy required to "prepare" the ligand for complex formation with $Cr(CO)_5$, by exposing the binding site, should vary in the same direction as the attractive component of the van der Waals interaction with $Cr(CO)_5$ once complex formation has occurred. While the magnitude of the contribution from the solvent term will in general not be the same as for $Cr(CO)_5$, the attractive van der Waals terms in the complex might be partially countered by corresponding terms in the ligand-solvent interaction. In this case, experimental measures of the enthalpies of ligand interactions with $Cr(CO)_5$ in solution would more strongly reflect changes in the repulsive van der Waals terms than do the computed values for total energy change. Experimental studies on both the gas-phase and solution systems could provide a test of this question. It should be kept in mind that the molecular mechanics model for a series such as under consideration here does not take account of variations in the metal-ligand bond strength occasioned by variations in ligand electronic properties. Thus, a comparison of the enthalpies of interaction of a series of phosphites with $Cr(CO)_5$ with the calculated values of $\Delta E_T$ would not be appropriate without taking account of variations in the strain-free donor character of the phosphites. This variation should be small for the acyclic trialkyl phosphites.

**Acknowledgment.** This research was supported by Grant CHE89-02773 from the National Science Foundation. BIOGRAF was made available through an academic grant from Molecular Simulation, Inc. The Stardent Titan computer on which the calculations were carried out was obtained through a University Research Initiative Award from the Defense Advanced Research Projects Agency. Much of the work was performed while M.L.C. was on sabbatical leave from Clarke College.

(27) Williams, J. E.; Stang, P. J.; Schleyer, P. v. R. *Annu. Rev. Phys. Chem.* **1968**, *19*, 531.

Contribution from the Department of Chemistry, School of Science and Engineering, Waseda University, Tokyo 169, Japan, and Department of Chemistry, Faculty of Science, Toho University, Funabashi, Chiba 274, Japan

# Synthesis, Crystal Structure, and Solvolysis Reaction of a H-T 3,3-Dimethylglutarimidate-Bridged Binuclear Platinum(II) Complex, $[Pt_2(NH_3)_4(C_7H_{10}NO_2)_2](NO_3)_2 \cdot H_2O$

Hiroshi Urata,[1a] Hiroshi Moriyama,[1b] and Kazuko Matsumoto*,[1a]

*Received September 10, 1990*

Synthesis and crystal structure of a 3,3-dimethylglutarimidate-bridged platinum complex (**1**) are reported. **1** is a binuclear structure with two 3,3-dimethylglutarimidate ligands bridging in a head-to-tail (H-T) manner. Each platinum atom is coordinated with two amine ligands in the cis position, a deprotonated nitrogen atom, and an oxygen atom of the 3,3-dimethylglutarimidate ligands. The Pt-Pt separation within the complex cation is 2.939 (1) Å. Although the $^{13}C$ spectrum of **1** in $D_2O$ measured immediately after dissolution corresponds to the solid structure, the spectrum gradually changes to an unknown one, which indicates that the binuclear structure is not stably retained in $D_2O$. From $^{13}C$ and $^{195}Pt$ NMR spectroscopy in $D_2O$ and DMSO-$d_6$, it turns out that the solvolysis reaction occurs in solution and the binuclear complex changes to a mononuclear one. Compound **1** crystallizes in the monoclinic space group $C2/c$ with $a$ = 36.933 (7) Å, $b$ = 10.473 (1) Å, $c$ = 14.070 (4) Å, $\beta$ = 105.28 (2)°, $V$ = 5249.8 (9) Å$^3$, and $Z$ = 8. Anisotropic refinement of all nonhydrogen atoms converged to the residuals $R$ = 0.059 and $R_w$ = 0.045 ($w = 1/\sigma^2(F)$).

## Introduction

Recently, amidate- or lactamate-bridged binuclear or tetranuclear platinum complexes have attracted the interest of many chemists because of the novel redox chemistry of these complexes involving the unusual Pt(III) oxidation state. Binuclear complexes of the formula $[Pt^{II}_2A_4L_2]^{2+}$ (A is $NH_3$ or (en)/2 and L is deprotonated amidate or lactamate ligand)[2-5] are oxidized to $[Pt^{III}_2A_4L_2XX']^{4+}$[6-8] (X and X' are axial ligands such as $NO_3^-$ or $NO_2^-$) or to tetranuclear mixed-valent platinum blues $[Pt^{II}_3Pt^{III}A_8L_4]^{5+}$[9-11] and platinum tans $[Pt^{II}_2Pt^{III}_2A_8L_4]^{6+}$.[12-14]

**Chart I**

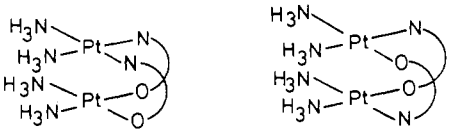

head-to-head (H-H) isomer head-to-tail (H-T) isomer

(1) (a) Waseda University. (b) Toho University.
(2) Hollis, L. S.; Lippard, S. J. *J. Am. Chem. Soc.* **1981**, *103*, 1230.
(3) Lippert, B.; Neugebauer, D.; Schubert, U. *Inorg. Chim. Acta* **1980**, *46*, L11.
(4) Hollis, L. S.; Lippard, S. J. *J. Am. Chem. Soc.* **1983**, *105*, 3494.
(5) Hollis, L. S.; Lippard, S. J. *Inorg. Chem.* **1983**, *22*, 2600.
(6) O'Halloran, T. V.; Roberts, M. M.; Lippard, S. J. *Inorg. Chem.* **1986**, *25*, 957.
(7) Hollis, L. S.; Lippard, S. J. *Inorg. Chem.* **1983**, *22*, 2605.
(8) Hollis, L. S.; Lippard, S. J. *J. Am. Chem. Soc.* **1981**, *103*, 6761.
(9) Lippert, B.; Schöllhorn, H.; Thewalt, U. *Inorg. Chem.* **1987**, *26*, 1736.
(10) Barton, J. K.; Szalda, D. J.; Rabinowitz, H. N.; Waszczak, J. V.; Lippard, S. J. *J. Am. Chem. Soc.* **1979**, *101*, 1434.
(11) Barton, J. K.; Caravana, C.; Lippard, S. J. *J. Am. Chem. Soc.* **1979**, *101*, 7269.
(12) Matsumoto, K.; Fuwa, K. *J. Am. Chem. Soc.* **1982**, *104*, 897.
(13) Matsumoto, K.; Takahashi, H.; Fuwa, K. *Inorg. Chem.* **1983**, *22*, 4086.

0020-1669/91/1330-3914$02.50/0 

Deprotonated amide nitrogen atoms, when coordinated to a metal, stablize higher oxidation states of the metal, which together with the tendency of platinum to form a Pt–Pt metal bonding at higher oxidation state leads to formation of the novel tetranuclear zigzag chain structures of platinum blues and tans.

The structures and solution properties of the amidate-bridged Pt(II) binuclear complexes $[Pt^{II}_2A_4L_2]^{2+}$ are considerably affected by the nature of the bridging amidate ligands. Novel isomerization between head-to-head (H–H) and head-to-tail (H–T) isomers (Chart I) has been reported for binuclear $[Pt^{II}_2A_4L_2]^{2+}$.[15-17] The isomerization rate in water is rather small ($k_f$ = 7.4 (2) × $10^{-5}$ and $k_r$ = 13.9 (2) × $10^{-5}$ $s^{-1}$) for the complex with A = $NH_3$ and L = α-pyridonate,[15] whereas it is fairly large and the equilibrium is reached almost instantaneously on dissolution when L is α-pyrrolidonate.[17] In the present study, the H–T 3,3-dimethylglutarimidate- (DMGI-) bridged dimer $[Pt_2(NH_3)_4(C_7H_{10}NO_2)_2](NO_3)_2 \cdot H_2O$ (**1**) has been synthesized and the crystal structure was solved. A $^{13}C$ and $^{195}Pt$ NMR study was undertaken

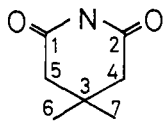


3,3-dimethylglutarimidate (DMGI)

to probe the H–T and H–H isomerization in solution; however, contrary to our expectation, the dimeric complex is solvolyzed into a monomeric complex with the coordinating amidate oxygen atom substituted by a solvent molecule.

## Experimental Section

**Synthesis of H–T $[Pt_2(NH_3)_4(C_7H_{10}NO_2)_2](NO_3)_2 \cdot H_2O$ (1).** The compound was prepared as follows. To a solution of *cis*-$Pt(NH_3)_2(OH_2)_2$ (1 mmol in 10 mL of $H_2O$), which was prepared by adding 2 equiv of $AgNO_3$ to *cis*-$Pt(NH_3)_2Cl_2$ and filtering off AgCl, was added 4 mmol of 3,3-dimethylglutarimide, and the pH of the solution was adjusted to 7 with 1 M NaOH. After the solution was heated at 90 °C for 3 h, the color of the solution turned to yellow. It was cooled with ice–water for 1 h, and the unreacted ligand was precipitated and was removed by filtration. To the yellow filtrate was added 0.8 g of $NaNO_3$, and the solution was left at room temperature for 2–3 days. Yellow plate crystals of **1** were obtained.

The compound was also prepared by reacting 1 mmol of *cis*-$Pt(NH_3)_2Cl_2$ with 2 mmol of 3,3-dimethylglutarimide in 25 mL of $H_2O$ at pH 9. The solution was heated at 60 °C until all the materials were dissolved. After further reaction for 1 h, 2.0 mmol of $AgNO_3$ was added and AgCl was removed by filtration. The solution was left at room temperature for 24 h and was condensed to 10 mL. Yellow microcrystals of **1** were obtained. Anal. Calcd for $[Pt_2(NH_3)_4(C_7H_{10}NO_2)_2](NO_3)_2 \cdot H_2O$: C, 19.09; H, 3.89; N, 12.73. Found: C, 19.16; H, 4.02; N, 12.73. The yield was 30%.

**Synthesis of *cis*-$[Pt(NH_3)_2(C_7H_{10}NO_2)(DMSO)](NO_3)$ (2).** Compound **2** was obtained by drying a DMSO solution of **1** under reduced pressure and was recrystallized from water. Anal. Calcd for $Pt(NH_3)_2(C_7H_{10}NO_2)(DMSO)](NO_3)$: C, 21.21; H, 4.26; N, 11.00. Found: C, 21.05; H, 4.26; N, 10.86.

**Synthesis of $[Pt_4(NH_3)_8(C_7H_{10}NO_2)_4](NO_3)_5 \cdot 2H_2O$ (3).** The compound was prepared by heating 10 mL of a $H_2O$ solution containing 1.0 mmol of *cis*-$Pt(NH_3)_2CL_2$ and 2.0 mmol of $AgNO_3$ at 60 °C for 2 h. AgCl was removed, and 4.0 mmol of 3,3-dimethylglutarimide was added to the filtrate. After the pH was adjusted to 7 with 1 M NaOH, the solution was heated at 80 °C for 2 h and then was cooled and the unreacted ligand was precipitated and removed by filtration. Nitric acid (0.8 mL) was added to the filtrate, and $O_2$ was bubbled through the solution until it turned dark blue. The solution gave blue rectangular plate crystals, after it was left standing at 30 °C for 2 days. Anal. Calcd for $[Pt_4(NH_3)_8(C_7H_{10}NO_2)_4](NO_3)_5 \cdot 2H_2O$: C, 18.44; H, 3.73; N, 13.06. Found: C, 18.64; H, 3.76; N, 12.96. Compound **3** was also obtained by slow evaporation of the filtrate of **1** at room temperature.

**Table I.** Crystallographic Data for $[Pt_2(NH_3)_4(DMGI)_2](NO_3)_2 \cdot H_2O$

| | |
|---|---|
| chem formula: $Pt_2C_{14}H_{34}N_8O_{11}$ | $Z$ = 8 |
| fw = 880.7 | $T$ = 23 ± 1 °C |
| cryst syst: monoclinic | λ = 0.710 69 Å |
| space group: $C2/c$ (No. 15) | $\rho_{obsd}$ = 2.23 g $cm^{-3}$ |
| $a$ = 36.933 (7) Å | $\rho_{calcd}$ = 2.21 g $cm^{-3}$ |
| $b$ = 10.473 (1) Å | $\mu$ = 108.22 $cm^{-1}$ |
| $c$ = 14.070 (4) Å | range transm factors = 1.00–0.57 |
| β = 105.28 (2)° | $R$ = 0.059 |
| $V$ = 5249.8 (9) Å$^3$ | $R_w$ = 0.045 ($w = 1/\sigma^2(F)$) |

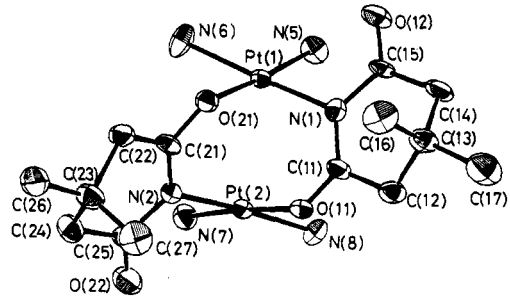


**Figure 1.** ORTEP drawing of H–T $[Pt_2(NH_3)_4(C_7H_{10}NO_2)_2]^{2+}$. Thermal ellipsoids are drawn at 50% probability.

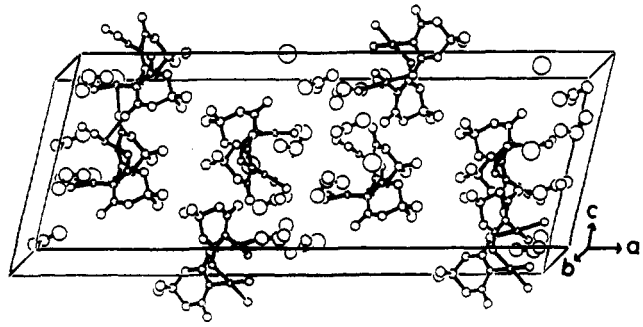


**Figure 2.** Crystal packing of H–T $[Pt_2(NH_3)_4(C_7H_{10}NO_2)_2](NO_3)_2 \cdot H_2O$ drawn with the ORTEP program.[20]

**Collection and Reduction of X-ray Data.** Compound **1** was subjected to a single-crystal X-ray study. Unit cell parameters were obtained from a least-squares fit of 21 reflections in the range 20° < 2θ < 25° measured on a Rigaku AFC-5R four-circle diffractometer with graphite-monochromated Mo Kα radiation. The details of the data collections are given in Table I and in supplementary Table S1.

**Solution and Refinement of the Structure.** The coordinates of the two independent platinum atoms were deduced from a Patterson map, and a series of block-diagonal least-squares refinements followed by a Fourier synthesis revealed all the remaining atoms except the hydrogen atoms. The structure was finally refined with anisotropic temperature factors for all of the non-hydrogen atoms to the final discrepancy index of $R$ = 0.059 and $R_w$ = 0.045, where $R = \sum||F_o| - |F_c||/\sum|F_o|$ and $R_w = [\sum w_i(|F_o| - |F_c|)^2/\sum w_i|F_o|^2]^{1/2}$ ($w_i = 1/\sigma^2(F)$). Atomic scattering factors and anomalous dispersion corrections were taken from ref 18. All the calculations were performed with the program system UNICS-III[19] and ORTEP.[20] Absorption correction was made by following the method of Busing et al.[21] No correction was made for extinction. None of the hydrogen atoms were located in the final difference map, and therefore they were not included in the calculation.

(14) Matsumoto, K.; Takahashi, H.; Fuwa, K. *J. Am. Chem. Soc.* **1984**, *106*, 2049.
(15) O'Halloran, T. V.; Lippard, S. J. *J. Am. Chem. Soc.* **1983**, *105*, 3341.
(16) O'Halloran, T. V.; Lippard, S. J. *Inorg. Chem.* **1989**, *28*, 1289.
(17) Matsumoto, K.; Miyamae, H.; Moriyama, H. *Inorg. Chem.* **1989**, *28*, 2959.
(18) *International Tables for X-ray Crystallography*; Kynoch Press: Birmingham, England, 1974; Vol. IV, pp 99, 149.
(19) Sakurai, T.; Kobayashi, K. *Rikagaku Kenkyusho Hokoku* **1979**, *55*, 69.
(20) Johnson, C. K. Report ORNL-3794 (revised); Oak Ridge National Laboratory: Oak Ridge, TN, 1976.
(21) Busing, W. R.; Levy, H. A. *Acta Crystallogr.* **1957**, *10*, 180.
(22) Lock, C. J. L.; Peresie, H. J.; Rosenberg, B.; Turner, G. *J. Am. Chem. Soc.* **1978**, *100*, 3371.
(23) Faggiani, R.; Lock, C. J. L.; Pollack, R. J.; Rosenberg, B.; Turner, G. *Inorg. Chem.* **1981**, *20*, 804.
(24) Faggiani, R.; Lippert, B.; Lock, C. J. L.; Speranzini, R. A. *J. Am. Chem. Soc.* **1981**, *103*, 1111.

**Table II.** Atomic Coordinates and Equivalent Thermal Parameters for **1**

| atom | *x* | *y* | *z* | $B_{eq}$,[a] Å$^2$ |
|---|---|---|---|---|
| Pt(1) | 0.09174 (2) | −0.20933 (8) | 0.42033 (4) | 2.79 (2) |
| Pt(2) | 0.09244 (2) | −0.28284 (8) | 0.62242 (4) | 2.78 (2) |
| N(1) | 0.1239 (4) | −0.3717 (13) | 0.4312 (10) | 3.3 (5) |
| O(11) | 0.1365 (4) | −0.3833 (11) | 0.6002 (8) | 4.4 (4) |
| O(12) | 0.1136 (4) | −0.3743 (14) | 0.2669 (8) | 5.1 (5) |
| C(11) | 0.1423 (6) | −0.4213 (18) | 0.5203 (12) | 3.7 (6) |
| C(12) | 0.1697 (6) | −0.5319 (19) | 0.5299 (13) | 4.4 (6) |
| C(13) | 0.1856 (5) | −0.5444 (20) | 0.4411 (13) | 4.7 (7) |
| C(14) | 0.1518 (6) | −0.5434 (20) | 0.3484 (13) | 5.1 (7) |
| C(15) | 0.1277 (5) | −0.4231 (18) | 0.3435 (11) | 3.3 (5) |
| C(16) | 0.2139 (7) | −0.4329 (24) | 0.4410 (18) | 6.5 (9) |
| C(17) | 0.2048 (7) | −0.6778 (25) | 0.4511 (17) | 7.8 (10) |
| N(2) | 0.1246 (4) | −0.1214 (13) | 0.6529 (9) | 3.0 (4) |
| O(21) | 0.1374 (3) | −0.1102 (11) | 0.5006 (8) | 3.4 (4) |
| O(22) | 0.1147 (4) | −0.1133 (14) | 0.8033 (9) | 5.8 (5) |
| C(21) | 0.1429 (5) | −0.0703 (18) | 0.5892 (11) | 3.3 (5) |
| C(22) | 0.1703 (6) | 0.0363 (18) | 0.6126 (13) | 4.5 (7) |
| C(23) | 0.1882 (6) | 0.0514 (19) | 0.7261 (14) | 4.7 (7) |
| C(24) | 0.1547 (6) | 0.0507 (20) | 0.7739 (14) | 4.6 (7) |
| C(25) | 0.1314 (5) | −0.0659 (18) | 0.7469 (12) | 3.7 (6) |
| C(26) | 0.2095 (7) | 0.1775 (20) | 0.07438 (16) | 6.5 (9) |
| C(27) | 0.2143 (7) | −0.0612 (24) | 0.7676 (18) | 6.5 (9) |
| N(5) | 0.0462 (4) | −0.3049 (15) | 0.3326 (11) | 4.2 (5) |
| N(6) | 0.0634 (4) | −0.0353 (14) | 0.4061 (13) | 4.7 (6) |
| N(7) | 0.0483 (4) | −0.1936 (14) | 0.6555 (10) | 4.0 (5) |
| N(8) | 0.0633 (4) | −0.4538 (14) | 0.6023 (11) | 4.0 (5) |
| N(3) | 0.0368 (6) | 0.3642 (20) | 0.3683 (15) | 8.0 (8) |
| O(31) | 0.0328 (5) | 0.2495 (15) | 0.3554 (11) | 7.1 (6) |
| O(32) | 0.0159 (5) | 0.4384 (18) | 0.3935 (13) | 9.0 (8) |
| O(33) | 0.0617 (7) | 0.4153 (20) | 0.3389 (24) | 15.9 (15) |
| N(4) | 0.0309 (8) | −0.1286 (22) | 0.1006 (20) | 14.0 (13) |
| O(41) | 0.0280 (6) | −0.2496 (16) | 0.1018 (13) | 9.7 (8) |
| O(42) | 0.0625 (5) | −0.0905 (19) | 0.1070 (16) | 10.7 (9) |
| O(43) | 0.0222 (6) | −0.0955 (21) | 0.1728 (14) | 11.5 (9) |
| O(WAT) | 0.1053 (8) | 0.2603 (37) | 0.5333 (22) | 21.1 (17) |

[a] The equivalent isotropic displacement parameter is defined as $4/3[a^2B_{11} + b^2B_{22} + c^2B_{33} + ab(\cos\gamma)B_{12} + ac(\cos\beta)B_{13} + bc(\cos\alpha)B_{23}]$.

**Table III.** Interatomic Distances (Å)

| | | | |
|---|---|---|---|
| | Metal–Metal | | |
| Pt(1)–Pt(2) | 2.939 (1) | | |
| | Coordination Bond | | |
| Pt(1)–N(1) | 2.06 (1) | Pt(1)–O(21) | 2.05 (1) |
| Pt(1)–N(5) | 2.07 (1) | Pt(1)–N(6) | 2.09 (2) |
| Pt(2)–O(11) | 2.03 (1) | Pt(2)–N(2) | 2.05 (1) |
| Pt(2)–N(7) | 2.04 (2) | Pt(2)–N(8) | 2.07 (1) |
| | Ligand Geometry | | |
| N(1)–C(11) | 1.36 (2) | N(1)–C(15) | 1.39 (2) |
| O(11)–C(11) | 1.26 (2) | O(12)–C(15) | 1.18 (2) |
| C(11)–C(12) | 1.52 (3) | C(12)–C(13) | 1.52 (3) |
| C(13)–C(14) | 1.55 (2) | C(13)–C(16) | 1.57 (3) |
| C(13)–C(17) | 1.56 (3) | C(14)–C(15) | 1.53 (3) |
| N(2)–C(21) | 1.37 (2) | N(2)–C(25) | 1.41 (2) |
| O(21)–C(21) | 1.28 (2) | O(22)–C(25) | 1.23 (3) |
| C(21)–C(22) | 1.46 (3) | C(22)–C(23) | 1.57 (2) |
| C(23)–C(24) | 1.55 (3) | C(23)–C(26) | 1.52 (3) |
| C(23)–C(27) | 1.54 (3) | C(24)–C(25) | 1.49 (3) |
| | Anion Geometry | | |
| N(3)–O(31) | 1.22 (3) | N(3)–O(32) | 1.21 (3) |
| N(3)–O(33) | 1.22 (4) | N(4)–O(41) | 1.27 (3) |
| N(4)–O(42) | 1.21 (3) | N(4)–O(43) | 1.19 (4) |

The final positional and thermal parameters are listed in Table II. The anisotropic temperature factors (Table S2) and the observed and calculated structure factors (Table S3) are available as supplementary material.

**NMR Measurements.** $^{13}$C NMR spectra were measured on a Bruker AC200P spectometer at 50.3 MHz, whereas $^{195}$Pt spectra were obtained on a Bruker AC300P spectrometer at 64.03 MHz. DMSO-$d_6$ solutions were prepared and measured at 25 °C. $^{13}$C chemical shift data are reported referenced to TMS, which is set in a sealed coaxial capillary tube in a 5-mm sample tube. For $^{195}$Pt chemical shift data, $H_2PtCl_6$ in $D_2O$ was used as the reference. All of the chemical shifts are expressed in ppm, and coupling constants, in Hz. Since the 90° pulse for $^{195}$Pt was 16 μs, a 25° pulse (4 μs) was adopted for accumulation.

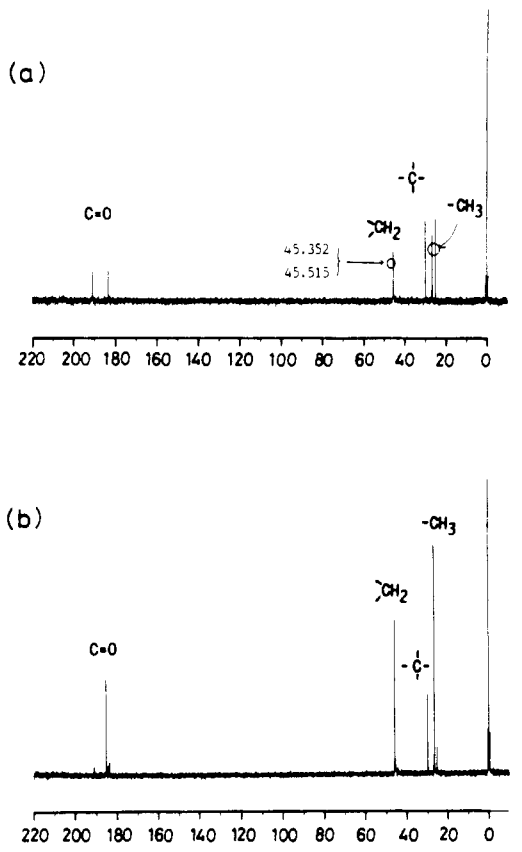


**Figure 3.** $^{13}$C NMR spectra of H–T $[Pt_2(NH_3)_4(C_7H_{10}NO_2)_2](NO_3)_2\cdot H_2O$ in $D_2O$: (a) spectrum immediately after dissolution; (b) spectrum 48 h after dissolution. The accumulation times were 3650 for spectrum a and 16 000 for spectrum b.

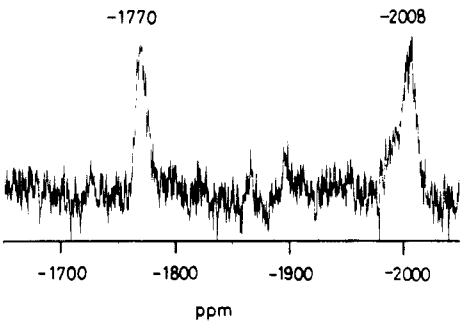


**Figure 4.** $^{195}$Pt NMR spectrum of H–T $[Pt_2(NH_3)_4(C_7H_{10}NO_2)_2](NO_3)_2\cdot H_2O$ in $D_2O$. The spectrum was measured immediately after dissolution with an accumulation time of 81 981.

**Electrochemical Measurements.** Cyclic voltammetry of **1** in 0.5 M $H_2SO_4$ was performed on a Fuso 315A potentiostat with a glassy-carbon-disk working electrode and a platinum-wire counter electrode. All the measurements were performed with a three-electrode system by using a SCE as the reference electrode.

## Results

**Structure of Compound 1.** The structure of H–T $[Pt_2(NH_3)_4(C_7H_{10}NO_2)_2]^{2+}$ is depicted in Figure 1. The crystal packing is shown in Figure 2. The selected bond distances and angles are listed in Tables III and IV, respectively. The two platinum atoms in **1** are bridged by two DMGI ligands in a H–T manner. Amidate-bridged H–T binuclear Pt(II) complexes similar to **1** are also reported for α-pyridonate[2,4] as bridging ligands.

**NMR Spectra of 1.** $^{13}$C spectra of **1** in $D_2O$ measured immediately after dissolution and 48 h after dissolution are shown in Figure 3. Although the spectrum of a freshly prepared solution (Figure 3a) is consistent with the H–T dimeric structure, the

Table IV. Interatomic Angles (deg)

| | | | |
|---|---|---|---|
| Coordination Bond | | | |
| Pt(2)-Pt(1)-N(1) | 81.6 (4) | Pt(1)-Pt(2)-O(11) | 77.8 (3) |
| Pt(2)-Pt(1)-O(21) | 78.7 (3) | Pt(1)-Pt(2)-N(2) | 80.9 (4) |
| Pt(2)-Pt(1)-N(5) | 104.4 (4) | Pt(1)-Pt(2)-N(7) | 107.3 (4) |
| Pt(2)-Pt(1)-N(6) | 101.4 (5) | Pt(1)-Pt(2)-N(8) | 102.8 (5) |
| N(1)-Pt(1)-O(21) | 90.1 (5) | O(11)-Pt(2)-N(2) | 90.8 (6) |
| N(1)-Pt(1)-N(5) | 90.5 (6) | O(11)-Pt(2)-N(7) | 174.5 (5) |
| N(1)-Pt(1)-N(6) | 174.5 (7) | O(11)-Pt(2)-N(8) | 86.5 (6) |
| O(21)-Pt(1)-N(5) | 176.9 (6) | N(2)-Pt(2)-N(7) | 91.6 (6) |
| O(21)-Pt(1)-N(6) | 86.0 (5) | N(2)-Pt(2)-N(8) | 174.8 (5) |
| N(5)-Pt(1)-N(6) | 93.2 (6) | N(7)-Pt(2)-N(8) | 90.5 (6) |
| Ligand Geometry | | | |
| Pt(1)-N(1)-C(11) | 122 (1) | Pt(2)-N(2)-C(21) | 123 (1) |
| Pt(1)-N(1)-C(15) | 117 (1) | Pt(2)-N(2)-C(25) | 119 (1) |
| C(11)-N(1)-C(15) | 122 (1) | C(21)-N(2)-C(25) | 117 (1) |
| Pt(2)-O(11)-C(11) | 129 (1) | Pt(1)-O(21)-C(21) | 127 (1) |
| N(1)-C(11)-O(11) | 123 (2) | N(2)-C(21)-O(21) | 122 (2) |
| N(1)-C(11)-C(12) | 122 (2) | N(2)-C(21)-C(22) | 125 (1) |
| O(11)-C(11)-C(12) | 115 (1) | O(21)-C(21)-C(22) | 117 (2) |
| C(11)-C(12)-C(13) | 116 (2) | C(21)-C(22)-C(23) | 112 (2) |
| C(12)-C(13)-C(14) | 107 (2) | C(22)-C(23)-C(24) | 106 (2) |
| C(12)-C(13)-C(16) | 110 (2) | C(22)-C(23)-C(26) | 108 (2) |
| C(12)-C(13)-C(17) | 106 (2) | C(22)-C(23)-C(27) | 111 (2) |
| C(14)-C(13)-C(16) | 113 (2) | C(24)-C(23)-C(26) | 112 (2) |
| C(14)-C(13)-C(17) | 109 (2) | C(24)-C(23)-C(27) | 109 (2) |
| C(16)-C(13)-C(17) | 112 (2) | C(26)-C(23)-C(27) | 111 (2) |
| C(13)-C(14)-C(15) | 112 (2) | C(23)-C(24)-C(25) | 112 (2) |
| N(1)-C(15)-O(12) | 121 (2) | N(2)-C(25)-O(22) | 116 (2) |
| N(1)-C(15)-C(14) | 118 (1) | N(2)-C(25)-C(24) | 122 (2) |
| O(12)-C(15)-C(14) | 121 (2) | O(22)-C(25)-C(24) | 122 (2) |
| Anion Geometry | | | |
| O(31)-N(3)-O(32) | 128 (2) | O(41)-N(4)-O(42) | 114 (3) |
| O(31)-N(3)-O(33) | 117 (2) | O(41)-N(4)-O(43) | 104 (3) |
| O(32)-N(3)-O(33) | 114 (2) | O(42)-N(4)-O(43) | 108 (2) |

spectrum is changed after 48 h to an unknown one (Figure 3b). The $^{195}Pt$ NMR spectrum in $D_2O$ shown in Figure 4 also does not correspond to a simple H-T dimeric structure, indicating the H-T dimer is converted to other species. When the H-T dimer solution is allowed to stand for a long time, the $^{195}Pt$ signal at −1770 ppm gradually decreases, and after sufficient time (more than 2 days) the spectrum clearly shows only one signal at −2008 ppm. The signal at −1770 ppm is, as mentioned later in the Discussion, due to the H-T dimer (**1**), whereas the peak at −2008 ppm corresponds to the final product, *cis*-$[Pt(NH_3)_2(C_7H_{10}NO_2)(D_2O)]^+$. The $^{13}C$ spectrum of a freshly prepared DMSO-$d_6$ solution (Figure 5a) also differs from what is expected for a H-T structure, and the spectrum rather resembles the spectrum of a $D_2O$ solution measured 48 h after dissolution; i.e., both spectra show only a single carbonyl carbon. The $^{195}Pt$ NMR spectrum in DMSO-$d_6$ shows a single peak at −3133 ppm. Tables V and VI summarize the $^{13}C$ chemical shifts and their assignments in $D_2O$ and DMSO-$d_6$, respectively.

## Discussion

**Synthesis of 1 and Chemical Species in the Reaction Solution.** Although the present synthetic procedures described in the Experimental Section selectively affords **1**, the filtrate of **1** becomes dark blue after 48 h of reaction at room temperature. This coloring reaction is not reproducible; sometimes, the filtrate remains pale yellow even after 1 week. Effects of pH and $AgNO_3$ amount were examined; however, no definite reason was found for the lack of reproducibility. Dark blue crystals of **3** were obtained after addition of nitric acid to the blue filtrate. The elemental analysis and the dark blue color ($\lambda_{max}$ = 752.8 nm, $\epsilon$ = 5010 $M^{-1}$ $cm^{-1}$, and $\lambda_{max}$ = 491.8 nm, $\epsilon$ = 570 in 0.5 M $H_2SO_4$) undoubtedly show that platinum blue[9-11] is produced in the solution. Since platinum blue is formed through oxidation of a H-H Pt(II) complex, $[Pt_2(NH_3)_4(L)_2]^{2+}$,[8,17] the present experiment shows that, in the filtrate of **1**, the H-H dimer is present, which is gradually oxidized to a tetranuclear platinum blue. Although the NMR study of **1** indicates, as mentioned in the following paragraphs, no evidence of H-T to H-H isomerization in solution,

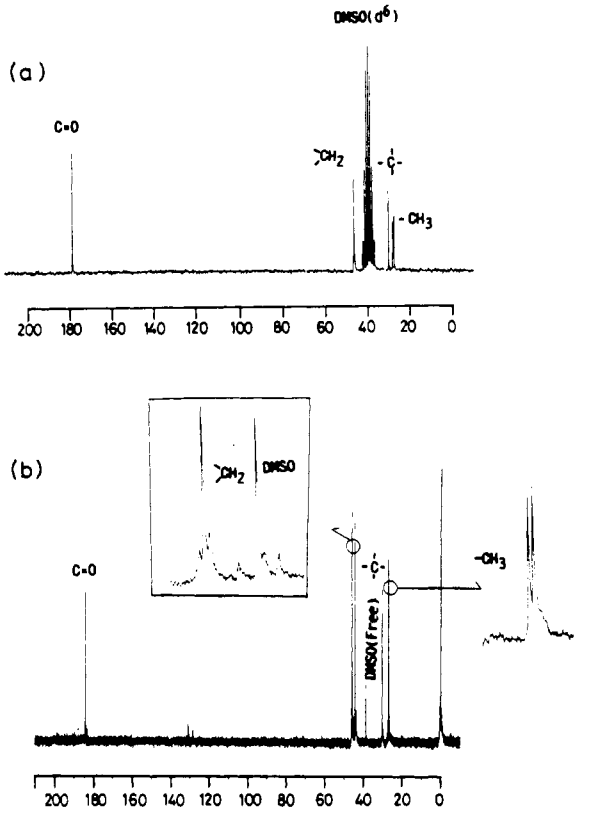


**Figure 5.** (a) $^{13}C$ NMR spectrum of H-T $[Pt_2(NH_3)_4(C_7H_{10}NO_2)_2](NO_3)_2 \cdot H_2O$ (**1**) in DMSO immediately after dissolution. (b) $^{13}C$ NMR spectrum of *cis*-$[Pt(NH_3)_2(C_7H_{10}NO_2)(DMSO)](NO_3)$ (**2**) in $D_2O$. The small peak at 38.8 ppm is free DMSO contained in the sample as impurity. The accumulation times were 1171 for spectrum a and 3702 for spectrum b.

which other amidate-bridged dimeric Pt(II) complexes show,[15-17] the H-H isomer of **1** seems to exist in the reaction solution. It is rather improbable that the H-T isomer directly becomes tetranuclear platinum blue on oxidation with simultaneous H-T to H-H isomerization. An aqueous acidic solution of **1** does not become dark blue even after a week of standing at room temperature. Several attempts were made to isolate the H-H isomer of **1**; however, all the efforts were in vain, and only the biue complex **3** was obtained.

**Crystal Structure of 1.** A comparison of the geometric features of thus far reported amidate-bridged H-T binuclear Pt(II) complexes is given in Table VII. The Pt-Pt distance (2.929 (1) Å) in the present complex is among the normal range for this class of complexes. Although the ligands of the previously reported complexes in Table VII all have aromatic rings and have shorter C-C distances compared with those in DMGI, the C-N and C-O distances and the O···N bite distances in coordination spheres (2.28 (2), 2.28 (2) Å) of the bridging DMGI and others are almost the same and there are no significant differences in the coordination distances around Pt atoms of these complexes. The dihedral angles and torsion angles in Table VII seem approximately a function of the Pt-Pt distances and both are larger as the Pt-Pt distance is longer. A stronger trans influence of the heterocyclic nitrogen atom compared to that of the carbonyl oxygen atom is manifested as longer Pt-N(ammine) distances trans to the heterocyclic nitrogen atoms (Pt(1)-N(6) (2.09 (2) Å > Pt(1)-N(5) (2.07 (1) Å) and Pt(2)-N(8) (2.07 (1) Å) > Pt(2)-N(7) (2.04 (2) Å). All of the coordination angles around each platinum atom are almost 90° with the deviations less than 4°. The deviations of the platinum atoms from their coordination planes, determined by least-squares refinement of the positions of the four coordination atoms, are comparable (Pt(1), 0.072 (8) Å; Pt (2), 0.079 (2) Å), and the direction of the displacement is toward the adjacent Pt atom in the complex.

All of the non-hydrogen atoms in DMGI, except the quaternary

**Table V.** $^{13}C$ NMR Data for $[Pt_2(NH_3)_4(C_7H_{10}NO_2)_2](NO_3)_2 \cdot H_2O$ Complexes and 3,3-Dimethylglutarimide in $D_2O$

| compound | chem shift, ppm | | | | | |
|---|---|---|---|---|---|---|
| | C1 | C2 | C4 | C5 | C3 | C6,7 |
| H–T 3,3-DMGI dimer (**1**) immediately after dissolution | 190.9 | 183.4 | 45.5 | 45.4 | 30.0 | 26.832<br>25.258 |
| H–T 3,3-DMGI dimer (**1**) 48 h after dissolution | 185.1 | | 45.8 | | 29.9 | 29.6 |
| 3,3-dimethylglutarimide | 176.9 | | 44.3 | | 29.8 | 26.6 |

**Table VI.** $^{13}C$ NMR Data for $[Pt_2(NH_3)_4(C_7H_{10}NO_2)_2](NO_3)_2 \cdot H_2O$, $[Pt(NH_3)_2(C_7H_{10}NO_2)(DMSO)](NO_3)$, and 3,3-Dimethylglutarimide in DMSO-$d_6$ and $D_2O$

| compound | chem shift (ppm) | | | | |
|---|---|---|---|---|---|
| | C1,2 | C4,5 | C3 | C6.7 | DMSO |
| H–T 3,3-DMGI dimer (**1**) in DMSO | 178.6 | 46.2 | 29.9 | 27.8<br>27.3 | |
| 3,3-dimethylglutarimide in DMSO | 172.7 | 44.8 | 29.5 | 27.0 | |
| $[Pt(NH_3)_2$(3,3-DMGI)-(DMSO)$](NO_3)$ (**2**) in $D_2O$ | 183.9 | 45.8 | 30.2 | 26.9<br>26.8 | 44.3 |
| 3,3-dimethylglutarimide in $D_2O$ | 176.9 | 44.3 | 29.8 | 26.6 | |

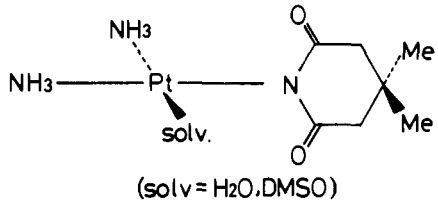


**Figure 6.** Solvolysis reaction of H–T $[Pt_2(NH_3)_4(C_7H_{10}NO_2)_2](NO_3)_2 \cdot H_2O$.

carbon and the two methyl groups bound to it, are coplanar. The DMGI rings are bent at the quaternary carbon, and the bending occurs in the direction so that the two quaternary carbon atoms of the two DMGI rings near each other when the complex is viewed along the Pt–Pt axis. The free carbonyl oxygen atom that does not participate in the platinum coordination lies above the platinum coordination plane and does not block the vacant axial position of the platinum atom.

The most significant changes in the geometry of the DMGI ring that accompany coordination occur in the bonds and angles at atoms adjacent to the Pt binding sites. A comparison of the bond angles of free DMGI to those in **1** shows a significant increase in the O(11)–C(11)–N(1) angle, from 119.4 (1) to 123 (2)°, and in the N(1)–C(11)–C(12) angle, from 117.3 (1) to 122 (2)°. These angle increases are accompanied by a decrease in the O(11)–C(11)–C(12) angle, from 123.4 (2) to 115 (1)°. The increase in the O(11)–C(11)–N(1) angle would be a result of bridging the large Pt–Pt distance, 2.939 (1) Å. The coordinating carbonyl C(11)–O(11) distance, 1.24 (2) Å, is significantly longer than those of the free ligand (1.225 (2) and 1.219 (2) Å), whereas the distance of the carbonyl C(15)–O(12) that does not participate in coordination is significantly shorter than those of the free ligand. The ring N(1)–C(11) distance is shorter than that of the free ligand, which is due to the multiplicity of the N(1)–C(11) bond. The above-mentioned tendency in the changes of bond angles and distances on coordination to the platinum atoms also applies to the other DMGI ligand in **1**.

The geometry of the nitrate anions is normal (Table III) and they link the binuclear cations through hydrogen bonds (Table S4).

**NMR Spectra and Solution Behavior of 1.** The $^{13}C$ and $^{195}Pt$ spectral changes of **1** after dissolution are explained by a solvolysis reaction of the H–T binuclear structure into a monomeric complex as shown in Figure 6. The more loosely coordinated exocyclic oxygen atom of the bridging DMGI in **1** is easily displaced by a solvent molecule and the monomeric complex *cis*-$[Pt(NH_3)_2$(DMGI)(solv)$]^+$ is produced. Figure 4 corresponds therefore to a 1:1 mixture of **1** (−1770 ppm) and the solvolysis product *cis*-$[Pt(NH_3)_2(DMGI)(D_2O)]^+$ (−2008 ppm). The reaction is much more rapid in DMSO than in $H_2O$, and the $^{13}C$ and $^{195}Pt$ spectra in DMSO (Figure 5a) indicate only the monomeric reaction product, even though the spectra are measured just after dissolution. The DMSO-coordinated monomeric complex **2** was isolated by dissolving **1** in non-deuterated DMSO as in the manner described in the Experimental Section. The $^{13}C$ NMR spectrum of **2** was measured in $D_2O$ and is shown in Figure 5b. The spectrum is identical with Figure 5a, except that coordinated DMSO is observed in $D_2O$ at 44.3 ppm with $^2J$(Pt–C) = 28.34 Hz. The spectrum in Figure 5a is therefore that of **2** in DMSO. The coordinated DMSO is not observed in DMSO-$d_6$, probably due to the exchange with the solvent and/or the weak intensity due to the multiple splitting of the coordinated DMSO-$d_6$ molecule.

From the fact that a single carbonyl peak and two DMGI methyl peaks are observed in Figure 5a, the DMGI ligand in the monomeric complex **2** is coordinated to the platinum atom at the endocyclic nitrogen atom and the amidate ligand is not rotated around the Pt–N bond. The two carbonyl groups are in the plane perpendicular to the platinum coordination plane, and thus the two carbonyl groups are equivalent. From Figure 5b it is evident that the DMSO molecule in **2** coordinates to the platinum atom by the sulfur atom and that the vector connecting the two methyl groups is perpendicular to the platinum coordination plane or the DMSO molecule is rotated around the Pt–S bond. In either case, the two methyl groups of DMSO are equivalent and appear as a single peak in Figure 5b. The evidence for the sulfur coordination of DMSO is also provided by the $^{195}Pt$ chemical shfit of **2** (−3133 ppm). Comparison of the $^{195}Pt$ chemical shifts of *cis*-$[Pt(NH_3)_2(H_2O)_2]^{2+}$ (−1593 ppm)[25] and *cis*-$[Pt(NH_3)_2$-

**Table VII.** Comparison of Geometric Properties of Related Platinum H–T Dimers

| compound | Pt–Pt dist, Å | dihedral angle,[a] deg | | ref |
|---|---|---|---|---|
| | | $\tau$ | $\omega$ | |
| $[Pt_2(NH_3)_4(C_7H_{10}NO_2)_2](NO_3)_2 \cdot H_2O$<br>L = 3,3-dimethylglutarimidate | 2.939 (1) | 35.2 | 21.3 | this work |
| $[Pt_2(NH_3)_4(C_5H_4NO)_2](NO_3) \cdot 2H_2O$<br>L = α-pyridonate | 2.8981 (5) | 28.8 | 13.0 | 4 |
| $[Pt_2(NH_3)_4(C_6H_7N_2O_2)_2[(NO_3)_2 \cdot H_2O$<br>L = 1-methylthyminate | 2.974 (1) | 36.1 | 13.8 | 22 |
| $[Pt_2(NH_3)_4(C_5H_5N_2O_2)_2](NO_3)_2 \cdot 3H_2O$<br>L = 1-methyluracilate | 2.954 (2) | 35.8 | 19.1 | 23 |
| $[Pt_2(NH_3)_4(C_5H_6N_3O)_2](NO_3)_2 \cdot 2H_2O$<br>L = 1-methylcytosinato | 2.981 (2) | 34 | 16 | 24 |

[a] $\tau$ is the tilt angle between adjacent platinum coordination planes in the binuclear unit, and $\omega$ is the average torsion angle about the Pt–Pt vector.

Table VIII. $^{195}Pt$ NMR Chemical Shifts (ppm) of H-T Amidate-Bridged Dimer and Monomer Complexes

| compound | coord sphere | chem shift, ppm | ref |
|---|---|---|---|
| H-T $[Pt_2(NH_3)_4(DMGI)_2](NO_3)_2$ (1) | $N_3O$ | -1770 | this work |
| *cis*-$[Pt(NH_3)_2(DMGI)(H_2O)]^+$ | $N_3O$ | -2008 | this work |
| H-T $[Pt_2(NH_3)_4(\alpha\text{-pyridone})_2](NO_3)_2$ | $N_3O$ | -1810 | 4 |
| *cis*-$[Pt(NH_3)_2(\alpha\text{-pyridone})(H_2O)]^+$ | $N_3O$ | -2015 | 4 |
| H-T $[Pt(NH_3)_2(\alpha\text{-pyrrolidone})_2]^{2+}$ | $N_3O$ | -1940 | 17 |
| *cis*-$[Pt(NH_3)_2(DMGI)(DMSO)]^{2+}$ (2) | $N_3S$ | -3133 | this work |
| $[Pt(NH_3)_3(Me_2SO)]^{2+}$ | $N_3S$ | -3224 | 25 |
| *cis*-$[Pt(^{15}NH_3)_2(H_2O)_2]^{2+}$ | $N_2O_2$ | -1593 | 25 |
| *cis*-$[Pt(^{15}NH_3)_2(DMSO)(H_2O)]^{2+}$ | $N_2OS$ | -2813 | 25 |

$(DMSO)(H_2O)]^{2+}$ (-2813 ppm)[25] (Table VIII) indicates that substitution of a coordinated oxygen atom by a sulfur atom greatly displaces the chemical shift about -1300 ppm to higher field. The large high-field shift observed also in **2** strongly supports the sulfur coordination in **2**.

In $D_2O$, a similar solvolysis reaction occurs and a monomeric *cis*-$[Pt(NH_3)_2(C_7H_{10}NO_2)(H_2O)]^+$ is produced. However, unlike the case of DMSO, the coordinated DMGI rotates rapidly about the Pt-N bond, since only a single methyl $^{13}C$ peak is observed in Figure 3b. The difference of the rotational movement of the coordinated DMGI in DMSO and in $D_2O$ seems to stem from the difference of the bulkiness of the coordinated DMSO and $D_2O$ molecules. A DMSO molecule is considerably larger and therefore would hinder the free rotation of the adjacent DMGI molecule.

In other analogous amidate-bridged binuclear Pt complexes, $^{13}C$ and $^{195}Pt$ NMR measurements exhibit H-T and H-H isomerization in solution.[15-17] The present complex (**1**) does not undergo such isomerization; instead, it is solvolyzed to a monomer complex. The ease of the solvolysis reaction observed for **1** is probably due to the existence of the noncoordinating carbonyl group, which withdraws electrons from the amidate nitrogen atom and reduces electron density at the exocyclic oxygen atom coordinating to the Pt atom. Therefore, the coordinating oxygen atom becomes more easily displaced by other ligands, such as a solvent molecule. In $\alpha$-pyridonate and $\alpha$-pyrrolidonate ligands, whose analogous Pt(II) dimeric complexes exhibit only H-H to H-T isomerizaton, no such noncoordinating oxygen atom exists, and therefore the coordinating exocyclic oxygen atom would be more negatively charged and thus more favorable for coordination. This difference of the electron density and of the coordination ability of the carbonyl oxygen atoms in amidate ligands would be the cause of the different solution behaviors of amidate-bridged Pt(II) dimeric complexes. The cyclic voltammogram of **1** exhibits a quasi-reversible single redox wave at 0.665 V ($=(E_{pa} + E_{pc})/2$) vs SCE ($E_{pa}$ = 0.69 V and $E_{pc}$ = 0.64 V), which was confirmed by coulometry to correspond to a two-electron process, $[Pt^{III}_2(NH_3)_4(C_7H_{10}NO_2)_2L_2]^{n+} + 2e^- \rightleftarrows$ **1** (L is a solvent molecule or a counteranion). This potential is considerably higher than those of the previously reported analogous complexes with a $\alpha$-pyridonate[6] or a $\alpha$-pyrrolidonate[17] bridging ligand and is considered to reflect the fact that the electron-donating ability of the present ligand to a platinum atom is much decreased due to the electron-withdrawing nature of the noncoordinating oxygen atom.

**Acknowledgment.** We are indebted to the Ministry of Education, Science and Culture, Japan, for its financial support by a Grant-in-Aid for Scientific Research on the Priority Area of "Multiplex Organic Systems" (01649008). Thanks are also due to the Hayashi Memorial Trust for Female Natural Scientists for its financial support.

**Supplementary Material Available:** Details of the X-ray data collection (Table S1), anisotropic temperature factors (Table S2), the possible hydrogen bondings (Table S4), and the $^{195}Pt$ NMR spectrum (Figure S1) (6 pages); the observed and calculated structure factors (Table S3) (14 pages). Ordering information is given on any current masthead page.

(25) Appleton, T. G.; Clark, H. C.; Manzer, L. E. *Coord. Chem. Rev.* **1973**, *10*, 335.

Contribution from the Department of Chemistry, The Ohio State University, Columbus, Ohio 43210, Department of Chemistry, Ford Motor Company, P.O. Box 2053, Dearborn, Michigan 48121, and Institute of Inorganic Chemistry, University of Munich, Meiserstrasse 1, 8000 Munich 2, West Germany

# Structure and Bonding Trends in Two- and Three-Coordinate Boron Cations

William F. Schneider,[1] Chaitanya K. Narula,*[,2] Heinrich Nöth,*[,3] and Bruce E. Bursten*[,1]

*Received March 15, 1991*

The electronic structure of two- and three-coordinate boron cations has been investigated with ab initio Hartree-Fock methods. The calculations successfully reproduce known boron cation molecular structures and can be used to predict reasonable geometries for cations that have not been characterized crystallographically. Substituent effects in both normal covalent and dative bonds were studied via calculated hydrogenation and dissociation reaction energies along with standard charge distribution analysis. The relative importance of $\sigma$ and $\pi$ effects in covalent bonding is dependent upon overall molecular coordination number and charge, with two-coordinate borinium cations relying most heavily on ligand $\pi$-donor ability, three-coordinate neutral boranes dominated by the ligand electronegativity ($\sigma$-donor capability), and three-coordinate borenium cations representing a compromise between these two. Dative bonding in the borenium cations is controlled by completely different effects; borinium cations are hard acids and thus bond strongly to hard bases and weakly to soft bases.

The structural chemistry of mononuclear boron is similar to that of traditional transition-metal coordination compounds. The bonding in the latter is typically characterized in terms of a two-electron dative donation from a formally neutral or anionic ligand to a central metal atom. A similar analysis is possible for boron compounds. For instance, the distribution of electrons in a neutral homoleptic three-coordinate boron compound can be represented as $B^{3+}(R^-)_3$, in which three anionic R groups donate two electrons each to the central cation to form three dative R-B $\sigma$ bonds.[4] This complete charge separation does not accurately represent the bonding in either transition-metal or boron compounds, but it is suggestive of their reactivity and of possible variability in the coordination sphere. As with the transition-metal elements, we can envision a series of boron "coordination compounds" $BR_nL_m^{(3-n)+}$ that contain a variable number of neutral and anionic ligands (but with boron restricted to the +3 oxidation state). Such a coordination chemistry has been demonstrated for four-coordinate boron, for which all species ranging from $BL_4^{3+}$

(1) The Ohio State University.
(2) Ford Motor Co.
(3) University of Munich.

(4) Throughout this paper we will use R to denote a formally anionic two-electron donor, such as an alkyl, alkoxide, or amide, and L to denote a neutral two-electron donor, such as an amine, ether, or phosphine.

0020-1669/91/1330-3919$02.50/0 